

Toward a Unified Approach to the Crystal Chemistry of Aurivillius-Type Compounds.

I. The Structural Model

Ph. Boullay,¹ G. Trolliard, and D. Mercurio

Laboratoire de Sciences des Procédés Céramiques et Traitements de Surface (CNRS UMR6638), Université de Limoges, 123 Avenue Albert Thomas, F-87060 Limoges Cedex, France

and

J. M. Perez-Mato and L. Elcoro

Departamento de Física de la Materia Condensada, Facultad de Ciencias, Universidad del País Vasco, Apdo. 664, E-48080 Bilbao, Spain

Received July 24, 2001; in revised form October 17, 2001; accepted November 30, 2001

A generalized structural model of Aurivillius-type compounds is presented using a 4D superspace group analysis where Aurivillius structures are considered as cation-deficient perovskites with the general formula $AB_{1-x}O_3$. Being essentially composition independent, the model is valid for any Aurivillius-type compounds where x is the only composition-dependent parameter. The atomic domains representing the atoms in superspace are described by means of crenel functions. For any composition, the conventional space groups can be easily derived from a unique superspace group. This work is supported by a TEM investigation where the continuously variable character of the diffraction diagram indicates that the various stacking sequences can be interpreted in terms of a structural modulation over a common average structure. © 2002 Elsevier Science (USA)

Key Words: Aurivillius phases; intergrowth compounds; modulated structures.

1. INTRODUCTION

The so-called Aurivillius phases are a family of layered bismuth oxides known for 50 years (1). The structure of these compounds is usually described as resulting from the regular stacking of $[M_2O_2]$ slabs and perovskite-like $[A_{n-1}B_nO_{3n+1}]^{2-}$ blocks. The integer n corresponds to the number of sheets of corner-sharing BO_6 octahedra forming the perovskite blocks where the A site can be occupied by large 12-fold-coordinated cations such as Na^+ , K^+ , Ca^{2+} , Sr^{2+} , Ba^{2+} , Pb^{2+} , Bi^{3+} , or Ln^{3+} , and the B site by 6-fold-

coordinated cations such as Fe^{3+} , Cr^{3+} , Ti^{4+} , Nb^{5+} , or W^{6+} . While the perovskite blocks offer large possibilities in terms of compositional flexibility, the cation sites in the interleave $[M_2O_2]$ slabs are almost exclusively occupied by Bi^{3+} cations forming $[Bi_2O_2]^{2+}$ slabs, which is actually the distinctive structural feature of Aurivillius phases. Recent works have nevertheless suggested that Bi^{3+} can be partially replaced by other lone pair cations, such as Pb^{2+} (2) and Tl^+ (3), or even by cations such as Sr^{2+} and La^{3+} (4).

A large number of Aurivillius phases exhibit ferroelectric properties at room temperature and their structures all derive from a nonpolar high-temperature prototype structure (SG $I4/mmm$ for simple members with $a_p = b_p \sim 3.9 \text{ \AA}$). In recent years, the ferroelectric properties of these oxides have attracted interest and an extensive amount of work has been done toward the realization of thin films in view of their potential application in nonvolatile memories (FeRAM: ferroelectric random access memory). Regarding the crystallography of these compounds a series of accurate single-crystal X-ray studies of members $n = 1$ to 3 (5–8) have been reported and the spontaneous polarization observed in these materials is now believed to result mainly from the A -site cation displacement inside the perovskite blocks (9).

Besides the simple members, which have been reported for n values up to 5, various ordered intergrowths of Aurivillius phases have been prepared as macroscopic pure phases. The reported compounds always correspond to the regular intergrowth of n and $n + 1$ members such as $Bi_7Ti_4NbO_{21}$ (intergrowth “2 + 3,” i.e., $Bi_3TiNbO_9 +$

¹To whom correspondence should be addressed. Fax: +33 5 55 45 72 70. E-mail: philippe.boullay@unilim.fr.

$\text{Bi}_4\text{Ti}_3\text{O}_{12}$) or $M^{\text{II}}\text{Bi}_8\text{Ti}_7\text{O}_{27}$ (intergrowth “3+4,” i.e., $\text{Bi}_4\text{Ti}_3\text{O}_{12} + M^{\text{II}}\text{Bi}_4\text{Ti}_4\text{O}_{15}$). The structural aspects of such intergrowths were first investigated by transmission electron microscopy (TEM) [see (10) for $\text{Bi}_7\text{Ti}_4\text{NbO}_{21}$ and (11) for $M^{\text{II}}\text{Bi}_8\text{Ti}_7\text{O}_{27}$]. The frequent occurrence of stacking faults in the intergrowth sequence lets us assume that other ordered intergrowths with longer periods along the stacking direction might be obtained in suitable systems and under appropriate synthesis conditions. Various examples of layered compounds exhibiting a composition-dependent series of long period structures (LPS) can be found in crystalline solids. In the past decade progress has been achieved toward a generalized description of such systems as modulated structures where the whole range of observed structures could be described within a single model in the superspace (12). Recently this idea has been successfully applied in oxides with the structure determination of compounds of type $A_{1+x}\text{BO}_3$ (13, 14) or in the case of the compound series $\text{LaTi}_{1-x}\text{O}_3$ (15). From this perspective, we propose a reinvestigation of the Aurivillius phases as being part of a larger class of compounds, i.e., composition-dependent intergrowths corresponding to a *B*-site cation-deficient perovskite having the generalized formula $AB_{1-x}\text{O}_3$.

In the first part of this paper, a TEM investigation within the pseudo-binary system $\text{Bi}_3\text{TiNbO}_9\text{--Bi}_4\text{Ti}_3\text{O}_{12}$ will evidence the existence of LPS in Aurivillius phases. Based on this observation, we will present the general superspace model that we propose for the description of the Aurivillius-type compounds.

2. EXPERIMENTAL

2.1. Synthesis

Powder materials corresponding to intermediate compositions between $\text{Bi}_3\text{TiNbO}_9$ and $\text{Bi}_4\text{Ti}_3\text{O}_{12}$ were prepared either by a solid state reaction of the corresponding oxides (Bi_2O_3 , TiO_2 and Nb_2O_5) or by using preformed $\text{Bi}_3\text{TiNbO}_9$ and $\text{Bi}_4\text{Ti}_3\text{O}_{12}$ as precursors. They were mixed in stoichiometric amounts, pressed into pellets, and heated at 1050°C. Short (2 hours) or long (several days) thermal treatment as well as post-annealing did not change significantly the obtained material. In particular, it was not possible to obtain a single-phase powder because of the recurrent presence of lower parent members ($n=2$, $n=3$, or intergrowth “2+3”).

2.2. Electron Microscopy

The electron microscopy study was carried out with a JEOL 2010 microscope working at 200 kV and fitted with a double-tilt ($\pm 30^\circ$) rotating sample holder. Regarding sample preparation, two techniques were used to lower

the strong anisotropic character of the compounds, which prevents observation of the stacking sequence. One involves crushing a few crystals and dropping them onto a copper grid covered by glue. The other involves the synthesis of ceramic samples strongly oriented by “hot-forging” under uniaxial pressure. A transverse section of the ceramic is then cut out and thinned by mechanical polishing and subsequent ion beam milling.

3. ELECTRON MICROSCOPY INVESTIGATION WITHIN THE PSEUDO-BINARY SYSTEM $\text{Bi}_3\text{TiNbO}_9\text{--Bi}_4\text{Ti}_3\text{O}_{12}$

At present, three Aurivillius phases are known in this system: $\text{Bi}_3\text{TiNbO}_9$ ($n=2$), $\text{Bi}_4\text{Ti}_3\text{O}_{12}$ ($n=3$), and the intergrowth $\text{Bi}_7\text{Ti}_4\text{NbO}_{21}$ ($n=2+3$). For this last compound, our recent crystallographic study (16) has shown that its structure can be considered a juxtaposition of the two members $n=2$ and $n=3$, forming a sequence of perovskite blocks 2^13^1 . A TEM investigation on this compound reveals accordingly for all crystallites a long-range ordered intergrowth 2^13^1 reflecting the chemical composition, with very few local faults (16). The possibility to form other ordered intergrowths was tested on compositions corresponding to perovskite block sequences 2^23^1 and 2^13^2 . As mentioned previously, we were not able to obtain single-phase powders. Nevertheless, as illustrated in Figs. 1a and 1b, TEM images show that in both cases crystallites exhibiting complex ordered stacking sequences can be found. In Fig. 1b the block sequence 2^23^1 is observed as expected from the initial composition, while in Fig. 1a, corresponding to the second composition, a sequence $(23)^33^1$ with a significant excess of $n=3$ blocks with respect to the composition 2+3 can be seen. These observations evidence that, locally, sequences different from those known up to now can be stabilized. Similarly as for the $n=2+3$ member, these crystallites reflect a composition at a nanoscopic level through the formation of ordered intergrowths with global composition $p(\text{Bi}_3\text{TiNbO}_9) + q(\text{Bi}_4\text{Ti}_3\text{O}_{12})$ (for instance $p=3$, $q=4$ in Fig. 1a).

Electron diffraction patterns (EDPs) collected on various crystallites confirm that these observations can be associated with specific long period ordered intergrowths and not with stacking faults in a disordered $n=2+3$ intergrowth. Indeed very few EDPs reveal intense diffuse streaks, which would be correlated with the existence of a strong disorder. Most of them exhibit patterns with spots close to the ones observed for the ordered $n=2+3$ intergrowth, but with clear deviations of the spots spacing from simple rational fractions as illustrated in Fig. 2. To index properly these EDPs, we should consider the Aurivillius phases as modulated phases (commensurate or incommensurate). In this respect, one first has to find the basic cell on which the modulation is defined. This can be done by looking at common features in the EDP, even considering the case of a disordered material (Fig. 2f).

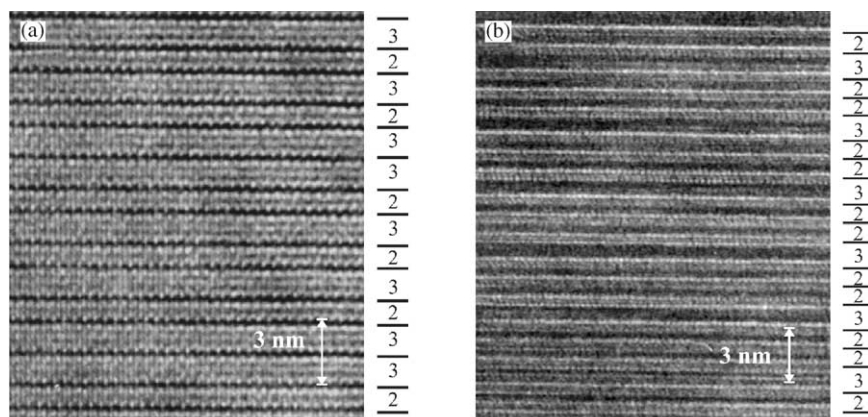


FIG. 1. HREM images showing evidence of stacking sequences for the perovskite blocks of the type 2^p3^q ($q > 1$ and/or $p > 1$) corresponding to an area with a composition $p(\text{Bi}_3\text{TiNbO}_9) + q(\text{Bi}_4\text{Ti}_3\text{O}_{12})$.

Clearly the spots indexed 006 for $n=2$, 008 for $n=3$, and 0014 for $n=2+3$ (Figs. 2a, 2b, and 2c, respectively) respond to that demand and in a superspace approach these reflections correspond to the same main reflection. In real space, this reflection is associated with a distance $1/s \approx 0.41$ nm (see Fig. 2c) corresponding approximately to the perovskite cell parameter a_p . It could be taken as the

average cell parameter along the z direction, with respect to which the modulation takes place. However, considering the A , B , and I centering respectively for $n=2$, $n=3$, and $n=2+3$, there is a systematic doubling of the periodicity along the z direction and one has to take twice this value. For the basic structure, the cell parameter along the z direction corresponds then to $c = 2a_p \approx 0.82$ nm with

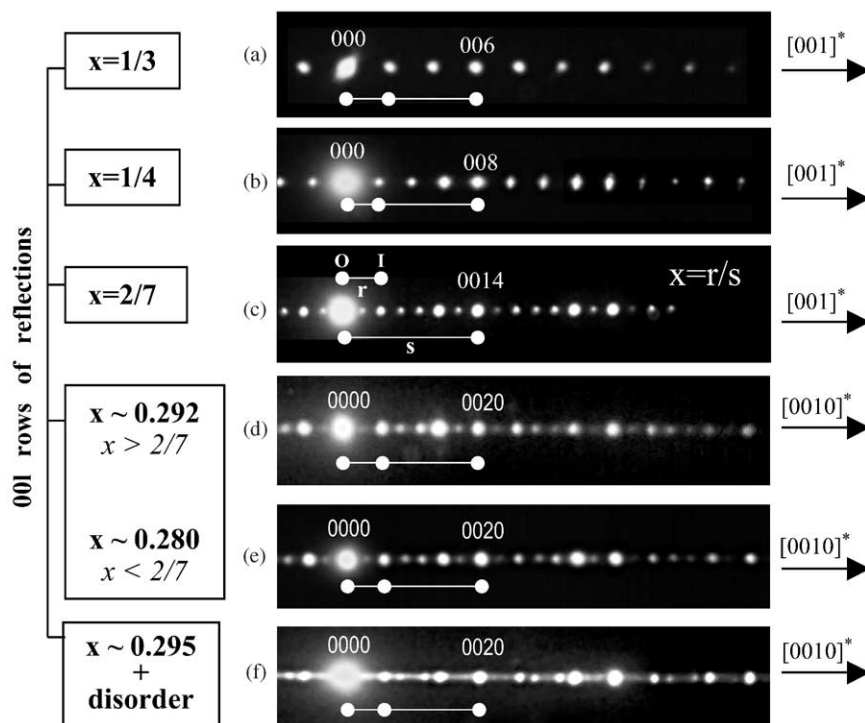


FIG. 2. $[001]^*$ (3D indexing) or $[0010]^*$ (4D indexing) rows of reflection as observed in electron diffraction patterns (EDPs) taken within the pseudo-binary system $\text{Bi}_3\text{TiNbO}_9\text{--Bi}_4\text{Ti}_3\text{O}_{12}$. (a, b, and c) EDPs for the monophasic compounds $\text{Bi}_3\text{TiNbO}_9$, $\text{Bi}_4\text{Ti}_3\text{O}_{12}$, and $\text{Bi}_7\text{Ti}_4\text{NbO}_{21}$, respectively. (d, e, and f) EDPs obtained for intermediate compositions (non-monophasic compounds) between $\text{Bi}_3\text{TiNbO}_9\text{--Bi}_7\text{Ti}_4\text{NbO}_{21}$ (d and f) and $\text{Bi}_7\text{Ti}_4\text{NbO}_{21}\text{--Bi}_4\text{Ti}_3\text{O}_{12}$ (e). For these three last EDPs, the indexation cannot be done using three indices and a modulation vector of the form $\mathbf{q} = x \cdot \mathbf{c}^*$ has to be used. Actually, using a vector of the form $\mathbf{g} = l\mathbf{c}^* + m\mathbf{q}$, the four indices indexation $00lm$ appears to be unique for all the EDPs.

$|\mathbf{c}^*| = s/2 \approx 1/(2 \times 0.41 \text{ nm})$. This means in the four indices indexation used in the superspace approach that this reflection will always be indexed as 0020, independently of the compound composition as indicated for the incommensurate cases in Figs. 2d to 2f. The “satellite” or “superstructure” reflections along the \mathbf{c}^* axis can be indexed using a vector of the form $l\mathbf{c}^* + m\mathbf{q}$, i.e., $00lm$. The choice of \mathbf{q} is in general not unique, especially in the commensurate cases (Figs. 2a to 2c), but usually there is a choice, which is more convenient for practical reasons. The strongest spots that are always present but whose positions change slightly with composition suggest this. A comparison of the different diffraction diagrams in Fig. 2 would in principle indicate that the segment OI of length r in Fig. 2c (and the analogous one for the other compositions) could be taken as the composition-dependent modulus of \mathbf{q} . However, as will be further developed, one can see in Fig. 3 that the $[00lm]^*$ rows of reflections have systematic extinctions so that r should be identified in fact with $2|\mathbf{q}|$. Hence, in terms of the reciprocal distances r and s shown in Fig. 2c, the chosen modulation wave vector is given in general by the relation $\mathbf{q} = (r/s)\mathbf{c}^*$, with $1/|\mathbf{c}^*| \approx 2 \times 0.41 \text{ nm}$. This relation can be compared with the usual estimate of the c parameter (c_n) of simple members of the family through the relation $c_n/2 \sim (n+1)0.41 \text{ nm}$, for a compound $A_{n+1}B_nO_{3(n+1)}$. This empirical expression indicates that the width of each basic unit of an Aurivillius compound is given approximately by $m = n+1$ perovskite unit-cell parameters, i.e., the actual number of octahedra layers within the perovskite block (n) plus an additional one corresponding to the thickness of the interleave $[\text{Bi}_2\text{O}_2]$ slab (about 0.45 nm). Hence, for $\text{Bi}_3\text{TiNbO}_9$ ($n=2$) and $\text{Bi}_4\text{Ti}_3\text{O}_{12}$ ($n=3$), $c_n/2$ corresponds to basic units with $m=3$ and $m=4$, i.e., $3a_p$ and $4a_p$ (see Fig. 3 part II as an illustration) and gives place to strong supercell spots corresponding to this distance, i.e., $r/s = 1/3$ and $1/4$, respectively, and in general $r/s = 1/(n+1)$.

In $\text{Bi}_7\text{Ti}_4\text{NbO}_{21}$ the more intense spot representative of the supercell (noted I in Fig. 2c) has intermediate positions, between those seen in $\text{Bi}_3\text{TiNbO}_9$ and $\text{Bi}_4\text{Ti}_3\text{O}_{12}$. The reciprocal of the distance $OI = r$ gives the average thickness of the basic unit of this compound, i.e., $7a_p$. Indeed, in the real space the value $s/r = 7/2 = 3.5$ represents the average number of perovskite unit cells in the period $c_{(2+3)}/2$, resulting from the intergrowth of $m=3$ and $m=4$ units. In general, r/s can be identified with the composition variable x in the formula $AB_{1-x}O_3$, when the compounds are expressed as cation-deficient perovskites. So, in general, $\mathbf{q} = x\mathbf{c}^*$. The variable x reduces to $1/(n+1)$ in the simple (non-intergrowth) members. We have then $\mathbf{q} = 1/3\mathbf{c}^*$ for $\text{Bi}_3\text{TiNbO}_9$, $\mathbf{q} = 1/4\mathbf{c}^*$ for $\text{Bi}_4\text{Ti}_3\text{O}_{12}$, and $\mathbf{q} = 2/7\mathbf{c}^*$ for $\text{Bi}_7\text{Ti}_4\text{NbO}_{21}$. The diffraction patterns in Figs. 2d and 2e remain globally of the same nature as the preceding ones

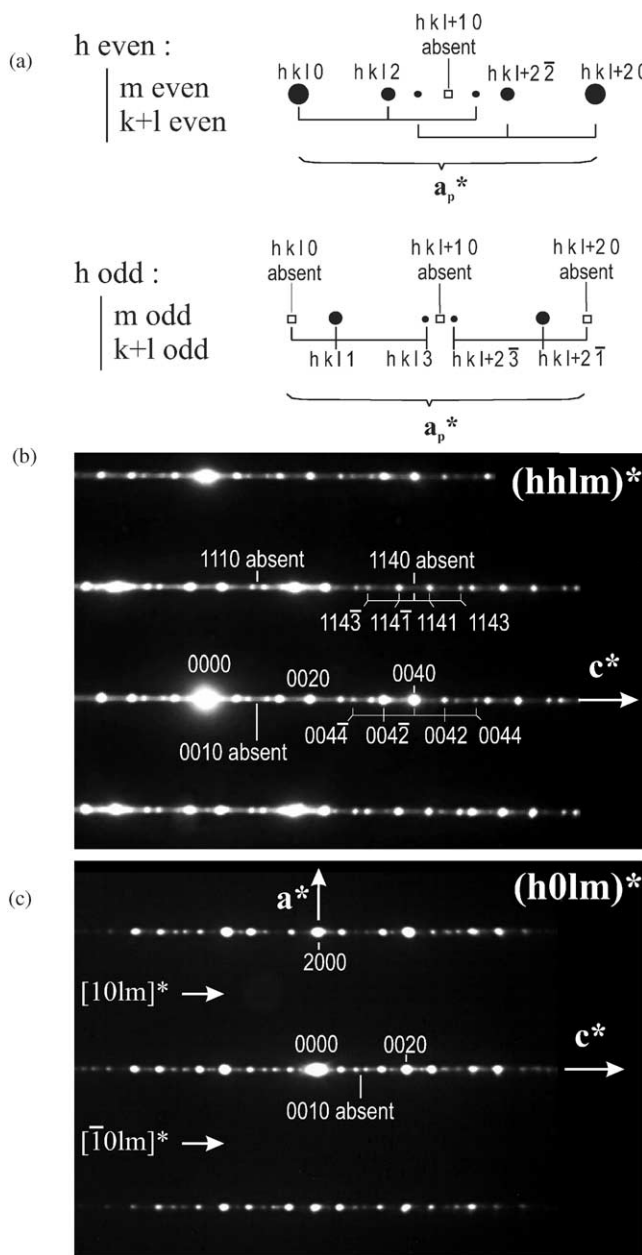


FIG. 3. (a) Scheme representing the principle for the four-indices indexation of reflections within the pseudo-binary system $\text{Bi}_3\text{TiNbO}_9$ – $\text{Bi}_4\text{Ti}_3\text{O}_{12}$. (b) Illustration of the indexation for an $(hhl m)^*$ plane observed in a disordered case. (c) The $[0100]$ zone axis EDP shows a condition for observed reflections in the plane $(h0lm)^*$ since for h odd the $[h0lm]^*$ rows of reflections are absent.

and we can keep assuming the relationship between composition and wave vector. The clear shift of the spot I indicates in these cases a more complex composition, with $x = r/s$ being a complex fraction with a large denominator or even in practice, and “incommensurate” number. They would correspond to intergrowths with a majority of $\text{Bi}_4\text{Ti}_3\text{O}_{12}$ units for $x < 2/7$ and a majority of $\text{Bi}_3\text{TiNbO}_9$

units for $x > 2/7$, as seen in the HREM images displayed in Fig. 1.

The following step is to index all the spots present in the EDPs recorded for various compounds. On the plane (x, y) , the unit cell parameters a and b used in the indexing correspond approximately to the translations $[1, \bar{1}, 0]_p$ and $[1, 1, 0]_p$ and therefore $a \sim b \sim \sqrt{2}a_p$. As stressed above, when the value $x = r/s$ is rational (as in Figs. 2a to 2c), the indexing along the \mathbf{c}^* axis might be ambiguous due to the overlapping of reflections, but the task is easier if one has cases where the value x is irrational as in Figs. 2d to 2f and one extrapolates from them. The principle used to index the EDP in 4D is schematized in the Fig. 3a and corresponds to the following observed reflection conditions on $hklm$: $h + k + l = 2n$ and $h + m = 2n$. As an illustration, an $(hhl m)^*$ plane observed for a disordered case is indexed in Fig. 3b. It is of importance to note that using this 4D approach and combining results for different compositions, the indexing of the spots becomes unambiguous. Apart from the above-mentioned general reflection conditions, an additional reflection condition is observed on the $[0100]$ zone axis patterns corresponding to $h0lm$: $m = 2n$ as illustrated in Fig. 3c.

From these observed reflection conditions, one can identify unambiguously the superspace group, common to the whole family of Aurivillius compounds, as $X2cm(00\gamma)000$, where X stands for a centered unit cell, which is nonconventional with respect to the tables of Janssen *et al.* (12) (see Table 1 for a complete definition of the superspace group including the centering translations). This group corresponds to the “conventional” $A2mm(1/2\ 0\ \gamma')0s0$ (no. 35.10) in the mentioned tables. This conventional setting for the superspace group corresponds to considering as average cell parameter along the x direction half the value of the one we use (i.e., $\mathbf{a}^* = 2\mathbf{a}^*$) with

$\gamma' = 1 - \gamma$. In this case the modulation wave vector corresponds to $\mathbf{q}' = 1/2\mathbf{a}'^* + \gamma'\mathbf{c}^*$, i.e., $\mathbf{q}' = \mathbf{a}^* + \mathbf{c}^* - \mathbf{q}$. In practice, it is more convenient to use the above nonconventional setting and eliminate the rational part of the modulation wave vector along the \mathbf{a} axis. Such nonconventional settings can be handled without problem by programs like JANA (17) and, thus, do not represent any additional difficulty in practice.

4. THE SUPERSPACE MODEL OF AURIVILLIUS PHASES

4.1. The Ideal Layer Model

The structure of the Aurivillius-type compounds consists of sheets of BO_6 octahedra stacked along the $\langle 001 \rangle$ direction of an ideal cubic perovskite structure (see Fig. 4a). As the width of the perovskite units or the number of layers in a period varies for different Aurivillius phases, the magnitude of the lattice parameter c is composition dependent. The two other orthogonal unit cell vectors span the octahedra layers and are practically composition independent. Characteristic of the Aurivillius phases, the occurrence of a $[Bi_2O_2]$ slab induces a shift $[\frac{1}{2}, \frac{1}{2}, 0]_p$ of the following layers of BO_6 octahedra in the stacking sequence.

As pointed out in the previous section, for the purpose of the superspace analysis, we will need to define first a structural model for which the above classic description is reduced to a modulation (in this case of occupation type) of a unique average cell. To start this superspace analysis, a suitable viewpoint is to describe the structure in terms of the stacking of individual layers instead of perovskite units. For the sake of simplicity, we will illustrate the layer model by considering the case of the paraelectric high-temperature phases with untilted octahedra (Fig. 4a). Starting with an ideal cubic perovskite ABO_3 , we consider along a $\langle 001 \rangle_p$ direction the regular stacking of AO and BO_2 layers. The $[Bi_2O_2]$ slabs in the Aurivillius structure can be seen as the result of a fault in the stacking of two successive AO layers (the mentioned $[\frac{1}{2}, \frac{1}{2}, 0]_p$ shift). The octahedral site suitable for the B cation of the interleave BO_2 layer does not exist anymore and the B cation is replaced by a vacancy resulting in a O_2 layer. The $A(Bi)$ cations of the two neighboring ($[\frac{1}{2}, \frac{1}{2}, 0]_p$ shifted) AO layers approach this anionic O_2 layer, forming the characteristic $[Bi_2O_2]$ slab. In another way, it can be said that if we associate an abstract spin up and down to unshifted and shifted AO layers, respectively (see Fig. 4b), the B vacancies occur when two successive AO layers have opposite “spin.” This description in real space is perfectly consistent with the conclusions made from the previous EDP analysis and we recover the description of a B -site-deficient perovskite $A(B_{1-x}\square_x)O_3$, where x represents the number of “faults” per perovskite unit. According to observations, these “faults” distribute along the stacking sequence in the most

TABLE 1
Symmetry Operations of the Superspace Group
 $X2cm(00x)000$ and Resulting Independent Reflection Conditions

Symmetry operations	
$\{E, 1 0\ 0\ 0, 0\}$	(x_1, x_2, x_3, x_4)
$\{2_x, -1 0\ 0\ 0, 2\phi\}$	$(x_1, -x_2, -x_3, -x_4 + 2\phi)$
$\{m_y, 1 0\ \frac{1}{2}\ 0, \frac{1}{2}\}$	$(x_1, \frac{1}{2} - x_2, x_3, \frac{1}{2} + x_4)$
$\{m_z, -1 0\ 0\ \frac{1}{2}, 2\phi\}$	$(x_1, x_2, \frac{1}{2} - x_3, -x_4 + 2\phi)$
$\{E, 1 \frac{1}{2}\ \frac{1}{2}, 0\}$	$(\frac{1}{2} + x_1, \frac{1}{2} + x_2, \frac{1}{2} + x_3, x_4)$
$\{E, 1 \frac{1}{2}\ 0\ 0, \frac{1}{2}\}$	$(\frac{1}{2} + x_1, x_2, x_3, \frac{1}{2} + x_4)$
$\{E, 1 0\ \frac{1}{2}\ \frac{1}{2}, \frac{1}{2}\}$	$(x_1, \frac{1}{2} + x_2, \frac{1}{2} + x_3, \frac{1}{2} + x_4)$
Reflection conditions	
$(hklm) h + m = 2n$	
$(hklm) h + k + l = 2n$	
$(h0lm) m = 2n$	

Note. In our case, $a \sim a_p\sqrt{2}$, $b \sim a_p\sqrt{2}$, $c \sim 2a_p$ and x is given by the composition variable in $AB_{1-x}O_3$.

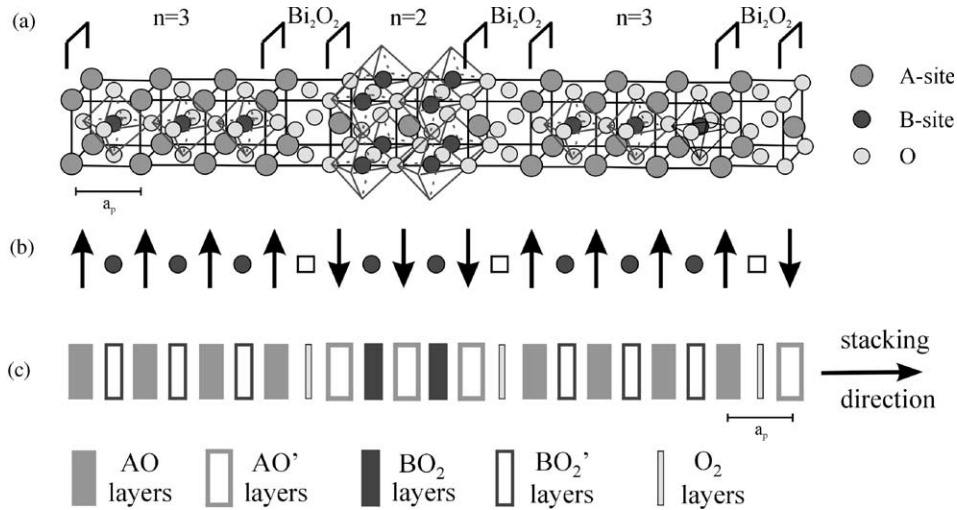


FIG. 4. Schematic of the layer model used in the modelisation of Aurivillius phases. (a) A “typical” representation where the $[\text{Bi}_2\text{O}_2]$ slabs are put apart from the perovskite blocks (p.b.) in the case here of a compound $\text{Bi}_7\text{Ti}_4\text{NbO}_{21}$ corresponding to a regular sequence of $|n=3 \text{ p.b.}[\text{Bi}_2\text{O}_2]|n=2 \text{ p.b.}[\text{Bi}_2\text{O}_2]$ along the stacking direction. Note that in this schematic drawing octahedra are untilted (high-temperature phase) for simplicity. (b) The occurrence of a $[\text{Bi}_2\text{O}_2]$ slab is directly associated with the stacking of two successive nonequivalent AO layers (shifted with respect to each other). (c) Following this idea, the stacking principle in Aurivillius phases can be modeled using five types of atomic layers. As a result, the $[\text{Bi}_2\text{O}_2]$ slabs are no longer considered as distinct from the perovskite blocks but rather as a consequence of structural shears in a perovskite-type structure.

uniform way compatible with the discreteness of the numbers involved, forming a so-called uniform sequence (18). Thus, the intergrowth $\text{Bi}_7\text{Ti}_4\text{NbO}_{21}$ ($n=2+3$) with $x=\frac{2}{7}$ reflects a uniform repartition of two “faults” into seven layers where the “faults” tend to be separated as far as possible, i.e., forming a 3^14^1 sequence of the unshifted and shifted AO layers (the sequence notation corresponds now to unshifted and shifted AO layers and not to perovskite blocks as in the previous section). Also, the more complex compositions observed by electron microscopy and discussed in the previous section exhibit uniform sequences of the $[\text{Bi}_2\text{O}_2]$ slabs. Starting from the regular stacking of AO and BO_2 layers, if we assume that this principle of uniform distribution of the “faults” has a general validity for any composition, the actual layer sequence for a given composition x can be directly derived from a Farey tree hierarchy (13) for the fraction x (Fig. 5). $\text{Bi}_3\text{TiNbO}_9$ ($x=1/3$) and $\text{Bi}_4\text{Ti}_3\text{O}_{12}$ ($x=1/4$) represent the two limit members of this tree. For instance, the uniform sequences observed in Fig. 1 are unambiguously determined by the corresponding composition x values (i.e., by the “fault” ratios) $7/25$ and $3/10$, respectively. Hence, as $x=3/10$ is obtained by the combination $3/10=1/3 \oplus 2/7=1/3 \oplus 1/3 \oplus 1/4$ the sequence is 3-3-4 or 3^24^1 (Fig. 1b). Similarly, for $x=7/25=2/7 \oplus 5/18=2/7 \oplus 2/7 \oplus 3/11=2/7 \oplus 2/7 \oplus 2/7 \oplus 1/4=1/3 \oplus 1/4 \oplus 1/3 \oplus 1/4 \oplus 1/3 \oplus 1/4 \oplus 1/4$, which would correspond to 3-4-3-4-3-4-4, or in short $(34)^34^1$ (Fig. 1a). We have thus obtained a way to describe any Aurivillius compound using five types of layers (see Fig. 4c). In general, $1/x$ represents the average

periodic distance, expressed in perovskite cell units, between consecutive “faults” or B vacancies along the stacking direction, and can be taken as the wavelength of the primary modulation over the perfect perovskite layer sequence, in other words $\mathbf{q}=x\mathbf{c}^*$. Hence, this simple layer model explains the direct relationship between composition and modulation vector observed in EDPs discussed above.

4.2. Superspace Description of the Aurivillius Phases

Regarding the transcription of the layer model into a superspace model, we can again start by considering the representation of a regular nonmodulated perovskite in the

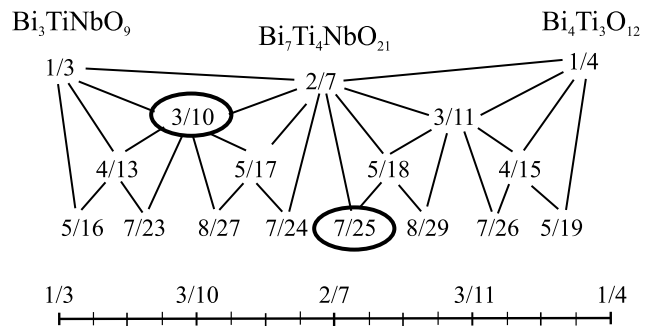


FIG. 5. Representation of the Farey tree series for the pseudo-binary system $\text{Bi}_3\text{TiNbO}_9$ – $\text{Bi}_4\text{Ti}_3\text{O}_{12}$ with the two limit members $x=1/3$ ($\text{Bi}_3\text{TiNbO}_9$) and $x=1/4$ ($\text{Bi}_4\text{Ti}_3\text{O}_{12}$). The members $x=3/10$ and $x=7/25$ correspond respectively to the sequences observed in Figs. 1b and 1a.

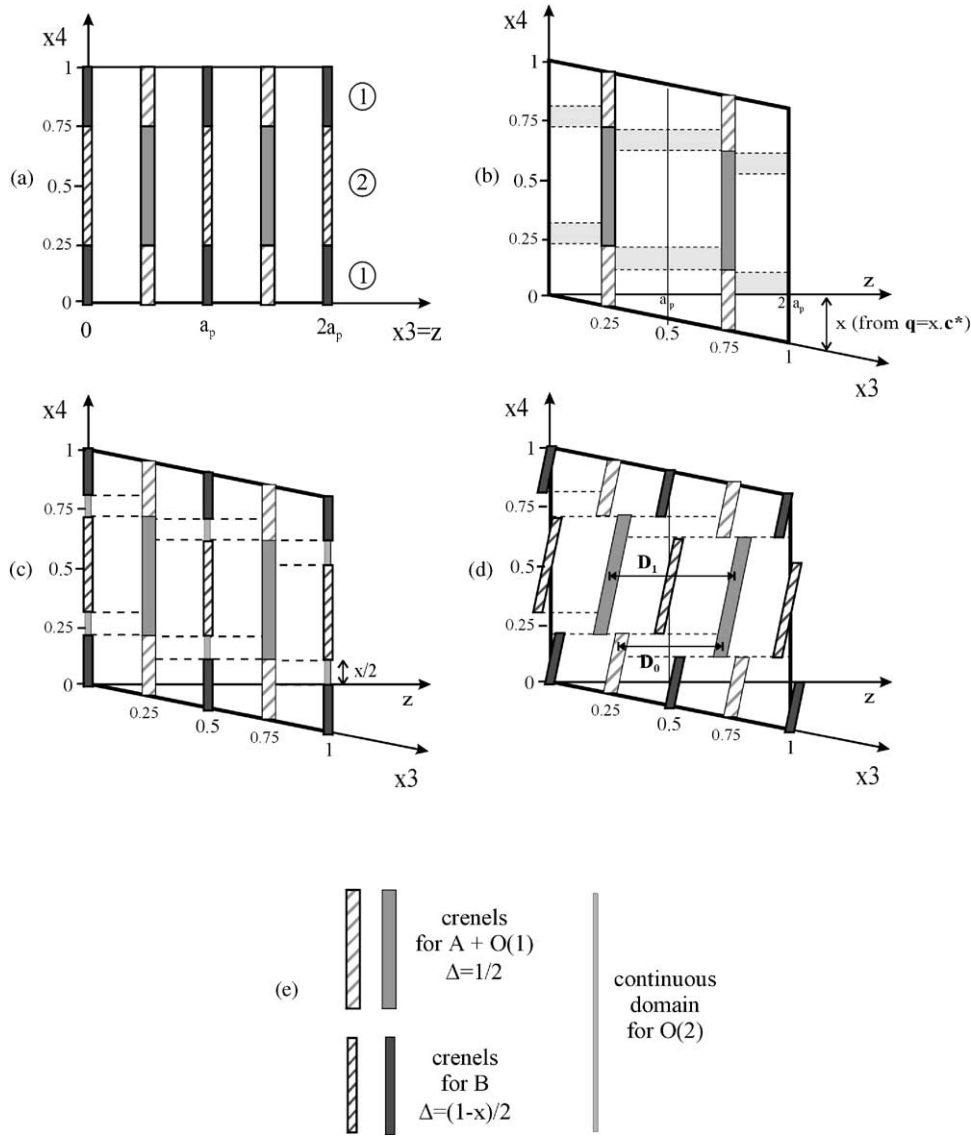


FIG. 6. Superspace construction for the generalized model of the Aurivillius phases. A stacking sequence along the z direction of the 3D physical space will be given by a cut perpendicular to the x_4 direction (a nonphysical internal dimension with arbitrary units). (a) Representation of a ABO_3 perovskite in a hypothetical superspace construction where no modulation vector is introduced. This perovskite has a periodicity of $2a_p$ along the stacking direction z . Along the x_4 direction, two stacking sequences shifted with respect to each other are used. (b) The introduction of a modulation vector in the form $\mathbf{q} = x.c^*$ generates the occurrence of the successive stacking of shifted AO atomic domains in certain zones (gray delimited) of the x_3 – x_4 section. (c) As illustrated in Fig. 4, for the zones located between two shifted A and $O(1)$ AD, the B AD should not exist and only $O(2)$ AD are still present. Thus a B -site-deficient perovskite $AB_{1-x}O_3$ is obtained. (d) The introduction of tilted AD gives rise to two different $[AO]$ – $[AO]$ interlayer distances, denoted D_0 and D_1 . Such tilting of AD can be modeled using sawtooth functions. (e) Symbolism used to represent the different AD. The Bi, Ti, and $O(1)$ AD have a limited extension Δ along the x_4 direction (crenel) while the $O(2)$ AD are continuous. Full and striped AD are used to indicate a different location along the $x_1 = x$ and $x_2 = y$ directions.

superspace, as illustrated in Fig. 6a. The periodicity along the x and y directions will correspond to the $a \sim \sqrt{2}a_p$ and $b \sim \sqrt{2}a_p$ parameters (case of the ferroelectric phases). The vertical axis represents the internal subspace whose periodicity is fixed arbitrarily (x_4 internal coordinate). The horizontal axis is the stacking direction (here z direction) whose periodicity corresponds to $2a_p$. In the construction of Fig. 6a, the atoms of the AO and BO_2

layers have crenel occupational domains along the internal space (further denoted AD for atomic domains). All those belonging to the same layer have equal z coordinates but different (x, y) coordinates. They therefore superpose in the figure and are schematized as single vertical bars. The layer sequence in the real space is obtained by means of a horizontal cut of the construction and the z coordinate in the 3D physical space will correspond to the x_3 coordinate

in the (3+1)D superspace. In the construction of Fig. 6a, depending on x_4 , we can only produce two sequences noted 1 and 2 which give equally a perovskite but whose (x, y) coordinates are $[\frac{1}{2}, 0] = [\frac{1}{2}, \frac{1}{2}]_p$ shifted with respect to each other.

The construction of Fig. 6a can be assimilated to the limit case ($x=0$) of the generalized description of Aurivillius structures as B -site-deficient perovskite. Actually, with such a construction, we have complicated the description of our simple perovskite and the added extra dimension appears useless. However, the point is that this description remains valid when a modulation vector $\mathbf{q} = x \cdot \mathbf{c}^*$ is added. As illustrated in Fig. 6b, for any horizontal cut, the layer sequence in real space is then modified and in particular successive shifted AO layers, i.e., “faults,” can be found in the sequence. As exposed in the layer model, this implies the existence of B vacancies. The two B crenel functions should reduce their length by $x/2$, corresponding to the regions along the internal coordinate, where two successive AO layers are shifted. As a result, we obtain the construction of Fig. 6c featuring AO , BO_2 , and O_2 layers present in the above layer model. The O_2 layers appear along the internal space as the result of the absence of B cations on the mentioned intervals of width $x/2$. Clearly a variation of x in $\mathbf{q} = x \cdot \mathbf{c}^*$ implies a modification of the occurrence of B vacancies in the sequence and of their total proportion. In fact, the superspace construction as shown in Fig. 6c implies a ratio of vacancies equal to x , i.e., a composition $AB_{1-x}O_3$, showing again the relationship between composition and modulation wave vector. By construction, for a given x , the actual sequence of B vacancies resulting from the model of Fig. 6c is the corresponding uniform sequence, which can be directly obtained using simple Farey tree rules as explained above.

The superspace construction is, however, not limited just to show the layers' sequence. Obviously, in a real system, A, O and B, O atoms are not located in the same (a, b) plane. The atomic deviations from these ideal layer plane positions can be described by displacive modulations leading to AD having a wavy form but with an extension limited along the internal direction by the crenel functions described in Fig. 6c. The superspace group of the structure restricts the form of these displacive modulations. A first-order approximation to these displacive modulations can be introduced by using tilted AD along the z direction, which gives rise to two different $[AO]$ - $[AO]$ interlayer distances depending on the interleave layer being BO_2 or O_2 as illustrated in Fig. 6d. Such tilting of AD can be modeled using sawtooth functions, as will be further detailed in the analysis of the experimental case (see part II in this issue).

An important step in the construction of the superspace model is to find the symmetry restrictions that will allow us to obtain the superspace group for the generalized model of

TABLE 2
Space Groups for Commensurate Structures with Rational x and Superspace Group $X2cm(00x)000$, Depending on the Parity of the Numerator n and Denominator p of x as a Function

$x = n / p$	$\phi = \text{arbitrary}$	$\phi = 0$ (mod. $1/2p$)	$\phi = 1/4p$ (mod. $1/2p$)
$n = \text{odd}$ $p = \text{odd}$	$A1a1$ SG no. 9	$A2aa$ SG no. 37	$A2_1am$ SG no. 36
$n = \text{odd}$ $p = \text{even}$	$B1a1$ SG no. 7	$B2ab$ SG no. 41	$B2am$ SG no. 39
$n = \text{even}$ $p = \text{odd}$	$I1c1$ SG no. 9	$I2cm$ SG no. 46	$I2cb$ SG no. 45

Aurivillius-type compounds. This is generally obtained by using information from X-ray, neutron, or electron diffraction experiments and also by checking consistency with previously refined structures in a 3D crystallographic approach. This work has been done in Section 3 by a close examination of various EDPs. In the results given in Table 1, some of the 4D symmetry operations contain a global phase ϕ . While arbitrary in an incommensurate structure, in the case of a commensurate modulation, it takes a fixed value, from which will depend the resulting conventional 3D space group symmetry. The possible 3D space groups for a given rational composition x can be obtained by applying simple algebraic rules (12) and are listed in Table 2. Knowing the value of x , this table allows to limit the choice of the 3D space group to only three possibilities that depend on the particular value of the phase ϕ , i.e., the section in superspace which corresponds to the real space structure. The right solution is obtained by examining experimental data in the course of the refinement of the structure. To our knowledge, all the Aurivillius phases reported to date belong to one of these nine predicted space groups. It is noticeable that the common single superspace group postulated for the whole family directly yields the alternative A or B centering observed in Aurivillius single block structures, depending on the parity of the perovskite blocks.

5. CONCLUSION

We have shown that the ferroelectric Aurivillius phases of the pseudo-binary system $\text{Bi}_3\text{TiNbO}_9$ - $\text{Bi}_4\text{Ti}_3\text{O}_{12}$ can all be described as modulated structures with a composition-dependent modulation wave vector. The corresponding superspace model is essentially composition independent and should be, in principle, valid for any ferroelectric Aurivillius-type compounds. Only the modulation wave vector and the composition-dependent width of the atomic occupation domains change with composition. For any composition, the conventional space groups can be easily derived from a unique superspace group. It was also shown

above that the superspace approach is especially well suited for properly describing in a unified form the ED observations done for samples of different compositions.

The layer model is not limited to the case of the ferroelectric phases and can be applied in a similar way to the high-temperature paraelectric phases using a different superspace group (nonpolar group), as will be shown in a forthcoming publication.

REFERENCES

1. B. Aurivillius, *Arkiv. Kemi* **1**, 463–480 and 499–512 (1949).
2. P. Millan and A. Castro, *Mater. Res. Bull.* **28**, 117 (1993).
3. P. Millan and A. Castro, *Mater. Res. Bull.* **34**, 25 (1999).
4. Ch. Hervoches and P. Lightfoot, *J. Solid State Chem.* **153**, 66 (2000).
5. A. D. Rae, J. G. Thompson, and R. L. Withers, *Acta Crystallogr. B* **47**, 870 (1991).
6. J. G. Thompson, A. D. Rae, R. L. Withers, and D. C. Craig, *Acta Crystallogr. B* **47**, 174 (1991).
7. A. D. Rae, J. G. Thompson, and R. L. Withers, *Acta Crystallogr. B* **48**, 418 (1992).
8. A. D. Rae, J. G. Thompson, R. L. Withers, and A. C. Willis, *Acta Crystallogr. B* **46**, 474 (1990).
9. R. L. Withers, J. G. Thompson, and A. D. Rae, *J. Solid State Chem.* **94**, 404 (1991).
10. S. Horiuchi, T. Kikuchi, and M. Goto, *Acta Crystallogr. A* **33**, 701 (1977).
11. D. A. Jefferson, M. K. Uppal, C. N. R. Rao, and D. J. Smith, *Mater. Res. Bull.* **19**, 1403 (1984).
12. T. Janssen, A. Janner, A. Looijenga-Vos, and P. M. de Wolff, "International Tables for Crystallography," Vol. C, Sect. 9.8. Kluwer Academic Publishers, Dordrecht, 1992.
13. J. M. Perez-Mato, M. Zakhour-Nakhl, F. Weil, and J. Darriet, *J. Mater. Chem.* **9**, 2795 (1999).
14. O. Gourdon, V. Petricek, M. Dusek, P. Bezdicka, S. Durovic, D. Gyepesova, and M. Evain, *Acta Crystallogr. B* **55**, 841 (1999).
15. L. Elcoro, J. M. Perez-Mato, and R. Withers, *Z. Kristallogr.* **215**, 727 (2000).
16. D. Mercurio, G. Trolliard, T. Hansen, and J. P. Mercurio, *Int. J. Inorg. Mater.* **2**, 397 (2000).
17. V. Petricek and M. Dusek, The Crystallographic Computing System JANA2000, Institute of Physics, Academy of Sciences of the Czech Republic, 2000.
18. S. Amelinckx and D. Van Dyck, "Electron Diffraction Techniques," Vol. 2, IUCr Monographs on Crystallography 4, p. 309. Oxford Univ. Press, London, 1993.